4-2014

Mechanism Underlying IKK Activation Mediated by the Linear Ubiquitin Chain Assembly Complex (LUBAC)

Hiroaki Fujita
Osaka University

Simin Rahighi
Chapman University, rahighi@chapman.edu

Mariko Akita
Osaka University

Ryuichi Kato
High-Energy Accelerator Research Organization (KEK)

Yoshiteru Sasaki
Kyoto University

See next page for additional authors

Recommended Citation

Hiroaki Fujita, Simin Rahighi, Mariko Akita, Ryuichi Kato, Yoshiteru Sasaki, Soichi Wakatsuki and Kazuhiro Iwai (2014). Mechanism underlying IKK activation mediated by the linear ubiquitin chain assembly complex (LUBAC). Mol. Cell Biol. 34 (7): 1322- 1335. doi: 10.1128/MCB.01538-13

Mechanism Underlying IKK Activation Mediated by the Linear Ubiquitin Chain Assembly Complex (LUBAC)

Authors
Hiroaki Fujita, Simin Rahighi, Mariko Akita, Ryuichi Kato, Yoshiteru Sasaki, Soichi Wakatsuki, and Kazuhiro Iwai

MCB Accepts, published online ahead of print on 27 January 2014
Mol. Cell. Biol. doi:10.1128/MCB.01538-13

TITLE

Mechanism underlying IKK activation mediated by the linear ubiquitin chain assembly complex (LUBAC)

Running title: Mechanisms of LUBAC-mediated NF-κB activation

Hiroaki Fujita[a, b, c], Simin Rahighi[d, e, 1], Mariko Akita[a], Ryuichi Kato[d], Yoshiteru Sasaki[c], Soichi Wakatsuki[d, e, f], and Kazuhiro Iwai[a, c, 1]

[a]Cell Biology and Metabolism Group, [b]Department of Frontier Biosciences, Graduate School of Frontier Biosciences, Osaka University, Suita 565-0871, Japan. [c]Department of Molecular and Cellular Physiology, Graduate School of Medicine, Kyoto University, Sakyo-ku, Kyoto 606-8501, Japan. [d]Structural Biology Research Center, Photon Factory, Institute of Materials Structure Science, High-Energy Accelerator Research Organization (KEK), Tsukuba, Ibaraki 305-0801, Japan. [e]Department of Structural Biology, Stanford University School of Medicine, Stanford, California 94305, USA. [f]SLAC National Accelerator Laboratory, Menlo Park, California 94025, USA.

[1]To whom correspondence may be addressed: E-mail: kiwai@mcp.med.kyoto-u.ac.jp or srahighi@stanford.edu.

Materials and methods: 2,118 words

Introduction, Results, and Discussion: 5,128 words

ABSTRACT

The LUBAC ubiquitin ligase complex, consisting of HOIL-1L, HOIP, and SHARPIN, specifically generates linear polyubiquitin chains. LUBAC-mediated linear polyubiquitination has been implicated in NF-κB activation. NEMO, a component of the IκB kinase (IKK) complex, is a substrate of LUBAC, but the precise molecular mechanism underlying linear chain-mediated NF-κB activation has not been fully elucidated. Here, we demonstrate that linearly polyubiquitinated NEMO activates IKK more potently than unanchored linear chains. In mutational analyses based on the crystal structure of the complex between the HOIP NZF1 and NEMO CC2-LZ domains, which are involved in the HOIP–NEMO interaction, NEMO mutations that impaired linear ubiquitin recognition activity and prevented recognition by LUBAC synergistically suppressed signal-induced NF-κB activation. HOIP NZF1 bound to NEMO and ubiquitin simultaneously, and HOIP NZF1 mutants defective in interaction with either NEMO or ubiquitin could not restore signal-induced NF-κB activation. Furthermore, linear chain-mediated activation of IKK2 involved homotypic interaction of the IKK2 kinase domain. Collectively, these results demonstrate that linear polyubiquitination of NEMO plays crucial roles in IKK activation, and that this modification involves the HOIP NZF1 domain and recognition of NEMO-conjugated linear ubiquitin chains by NEMO on another IKK complex. (191/200 words)

INTRODUCTION

Nuclear factor κB (NF-κB) is a family of transcription factors that play essential roles in many biological phenomena, including inflammatory responses, cell survival, and innate and acquired immune responses (1). Because aberrant activation of NF-κB signaling is associated with many pathological conditions, such as auto-inflammatory diseases and malignancies (2, 3), signal-induced activation of NF-κB has been studied extensively (4). In resting cells, inactive NF-κB resides in the cytoplasm bound to its inhibitor proteins, the inhibitors of κB (IκBs). Stimulation by inflammatory cytokines activates the IKK (IκB kinase) complex, composed of IKK1, IKK2, and NF-κB essential modulator (NEMO). Following phosphorylation by activated IKK, IκBs are degraded by the proteasome, leading to the release of NF-κB, which then translocates to the nucleus to induce transcription of its target genes (5).

The ubiquitin-conjugation system is deeply involved in the regulation of NF-κB pathway (6). Recent studies showed that the LUBAC ubiquitin ligase, which specifically generates linear polyubiquitin chains, is involved in NF-κB activation (7, 8). LUBAC is composed of three subunits: HOIP, HOIL-1L, and SHARPIN. Patients lacking HOIL-1L and mice lacking SHARPIN exhibit immunodeficiency and chronic inflammation, demonstrating the physiological significance of LUBAC-mediated linear polyubiquitination (9-12). In cells from mice lacking HOIL-1L or SHARPIN, the level of the residual LUBAC complex (consisting of the remaining two components) is reduced, and TNF-α–induced NF-κB activation is sharply attenuated (9-12).

Although NEMO is a target of linear polyubiquitination by LUBAC, it is not yet clear how linear polyubiquitination of NEMO triggers IKK activation.

In this study, using an *in vitro* LUBAC-mediated IKK activation assay, we found that linear diubiquitin conjugation to NEMO potently induces IKK activation. We then dissected the molecular mechanism underlying linear polyubiquitination of NEMO by LUBAC, and found that the NPL4 zinc finger 1 (NZF1) domain of HOIP is responsible for recognition of a region in the coiled-coil 2 and leucine zipper (CoZi) domains of NEMO. Mutational analyses based on a co-crystal structure of HOIP NZF1 and NEMO CoZi revealed that HOIP NZF1 binds to NEMO and ubiquitin simultaneously, and that both interactions are involved in linear polyubiquitination of NEMO, IKK activation, and subsequent activation of NF-κB. Finally, we showed that homodimerization of IKK2 is involved in linear ubiquitin chain-mediated IKK activation. Taken together, our results suggest that recognition of linear polyubiquitins conjugated to NEMO, possibly by NEMO in another IKK complex, triggers activation of IKK2 by *trans* auto-phosphorylation.

MATERIALS AND METHODS

RT-PCR and plasmids. The open reading frames of mouse HOIP and NEMO were amplified by RT-PCR of total RNA from C57BL/6 mouse liver. Other cDNAs used in this study were described previously (8, 12). The following full-length proteins, deletion mutants, and fragments were generated from the amplified ORF of HOIP: wild type (WT) (amino acids 1–1066), Δall-ZFs (deletion of 296–432), ΔZF (deletion of 296–325), ΔNZF1 (deletion of 344–373), ΔNZF2 (deletion of 402–432), and NZF1 (amino acids 344–382). The following proteins were generated from the amplified ORF of NEMO: WT (amino acids 1–412), ΔCoZi (deletion of 250–339), and ΔZF (amino acids 1–385). Mutants of HOIP (R369A, T354A, F355A, T354A/F355A), NEMO (Q271A, D275A, Q271A/D275A, K278R, K302R, K278R/K302R, Q271A/D275A/K278R/K302R, F305A, E313A, Q271A/D275A/F305A, Q271A/D275A/E313A) and IKK2 (V229A/H232A, Y294L/G295K/P296Q) were generated by two-step polymerase chain reaction (PCR). cDNAs were ligated to the appropriate epitope-tag sequences and then cloned into pcDNA3.1, pcDNA3.1-MMTV (8), pMAL-c2x (New England Biolabs), pGEX-6p1 (GE Healthcare), or MXs-IP (kindly provided by T. Kitamura). pGEX-IκBα (1–54) was described previously (8).

Antibodies and reagents. The following antibodies were used: FLAG (M2) (Stratagene); TNFR1

(ab19139) (Abcam); ubiquitin (sc-8017), HA (sc-805), Glutathione S-transferase (GST) (sc-459), maltose binding protein (MBP) (sc-13564), TRADD (sc-7868), and NEMO (sc-8330) (Santa Cruz Biotechnology); FLAG (F7425) (Sigma); T7 (69522) (Novagen); NEMO (K0159-3) (MBL); and pIKK1/2 (#2078), RIP1 (#3493), pIκBα (#9246), and IκBα (#4812) (Cell Signaling). His_6-HA-Ub_2, linear di- and tetra-ubiquitins and FLAG-His_6-TNF-α (FH-TNF-α) were expressed in *E. coli*. K63 diubiquitin and polyubiquitin chains ($Ub_{1–7}$, Lys63-linked) were purchased from Boston Biochem. Other antibodies and reagents were generated in our laboratory, as described previously (7, 8, 12).

Cell lines, cell cultures, and transfection. NEMO-deficient MEFs, N-1 cells (13), HEK293T cells, and HOIP Δlinear MEFs, which were established from mice that express a truncated HOIP (HOIP Δlinear) that lacks the C-terminal catalytic region, were grown in Dulbecco's modified Eagle's medium (DMEM) supplemented with 10% fetal bovine serum (FBS), 100 IU/ml penicillin, and 100 μg/ml streptomycin. NEMO-deficient MEFs were kindly provided by Dr. H. Kamata (Hiroshima University). NEMO-deficient MEFs stably expressing NEMO WT or mutants were selected with 150 μg/ml hygromycin B (Wako) after transfection with WT or mutant pcDNA3.1-MMTV-FLAG-NEMO constructs. N-1 cells stably expressing NEMO WT or mutants, and HOIP Δlinear MEFs stably expressing HOIP WT, ΔNZF1, R369A, or T354A/F355A, were generated using a retroviral expression system, as described previously (12); stable clones were

selected with 0.2 μg/ml puromycin (Sigma-Aldrich) or 500 μg/ml G418 (Nacalai Tesque). Transfections were performed using Lipofectamine 2000 (Invitrogen).

Immunoprecipitation and immunoblotting. Cells were lysed with lysis buffer containing 50 mM Tris-HCl (pH 7.5), 150 mM NaCl, 1% Triton X-100, 2 mM PMSF, and protease inhibitor cocktail (Sigma-Aldrich); lysates were clarified by centrifugation at 15,000 rpm for 20 min at 4°C. For hot lysis, cells were lysed with lysis buffer containing 1% SDS in phosphate-buffered solution (PBS), and then heated at 95°C for 10 min to disrupt non-covalent interactions. After heating, lysates were sheared with a 25G needle and centrifuged at 15,000 rpm for 5 min at room temperature; the resultant supernatant was diluted to 0.1% SDS with lysis buffer containing 50 mM Tris-HCl (pH 7.5), 150 mM NaCl, and 1% Triton X-100. For immunoprecipitations, lysates were incubated with the appropriate antibodies for 2 h on ice, and then immobilized on rmp–Protein A Sepharose beads (GE Healthcare). The beads were washed five times with buffer containing 50 mM Tris-HCl (pH 7.5), 150 mM NaCl, and 1% Triton X-100. In immunoprecipitations of HA-HOIP, to digest the polyubiquitin chains conjugated to NEMO, the beads were washed two more times with buffer containing 50 mM HEPES-HCl (pH 7.5) and 150 mM NaCl, and then incubated with 50 μg/ml UPS2cc (kindly provided by Dr. Rohan Baker (14)) for 1 h at 37°C in buffer containing 50 mM HEPES-HCl (pH 7.5), 150 mM NaCl, and 5 mM DTT. Samples were separated by SDS-PAGE and then transferred to PVDF membranes. After blocking in Tris-buffered saline (TBS) containing

133 0.1% Tween-20 and 5% (w/v) nonfat dry milk, the membranes were incubated with the appropriate
134 primary antibodies, followed by incubation with secondary antibodies. Membranes were
135 visualized using enhanced chemiluminescence and analyzed on a LAS4000mini (Fuji Film).
136
137 **Protein expression and purification.** GST-fused mouse HOIP (amino acids 344–382),
138 MBP-fused mouse NEMO (full-length), and mutants derived from either of these fusion proteins
139 were expressed in *E.* coli. Fusion proteins were purified using glutathione-Sepharose (GST-HOIP
140 and derivatives) or amylose resin (MBP-NEMO and derivatives). Recombinant E1, UbcH5c,
141 His_6-HOIP-HOIL-1L-Myc-SHARPIN complex, GST-IκBα (1–54), linear diubiquitin, and
142 tetra-ubiquitin were prepared, as described previously (7, 8, 15). IKK complex containing
143 HA-IKK1, IKK2, and FLAG-His_6-tagged NEMO (WT or R316A/R319A/E320A) were purified
144 using the baculovirus expression system. IKK complexes were prepared from High Five cells
145 infected with appropriate combinations of baculoviruses, and the complexes were then purified on
146 Ni-nitrilotriacetic acid (Ni-NTA) agarose. After incubation with Ni-NTA agarose, bead-bound
147 proteins were treated with 100 units of calf intestinal alkaline phosphatase (New England BioLabs)
148 for 30 min at 37°C; beads were washed with ten column volumes of 5 mM imidazole; and bound
149 proteins were eluted with 300 mM imidazole.
150 For crystallization, mouse NEMO CoZi (amino acids 250–339) and human HOIP NZF1
151 (amino acids 350–379) proteins were expressed and purified separately, and mixed at the proper

ratio immediately before crystallization (see next section). To generate expression constructs, NEMO CoZi was cloned into pGEX-4T-1 (GE Healthcare) and HOIP NZF1 was cloned into pGEX-6p-1. The resultant vectors were transformed into *E. coli* BL21, and overexpression of the GST-tagged proteins was induced by addition of 0.5 mM IPTG. After overnight incubation at 25°C, cells were collected and lysed by sonication. The supernatants were applied to glutathione-Sepharose 4B columns (GE Healthcare). The GST tags were cleaved using thrombin/PreScission protease, and proteins were eluted from the columns with PBS buffer. Further purification of the proteins was performed by gel-filtration chromatography in a buffer containing 150 mM NaCl and 50 mM Tris-HCl (pH 8.0).

Crystallization, data collection, and structure determination of the NEMO CoZi/ HOIP NZF1 complex. Immediately before crystallization, mNEMO CoZi and hHOIP NZF1 were mixed in a 2:1 molar ratio (the sequence similarity between human and mouse HOIP is illustrated in Fig. 3J). Co-crystals were obtained after 6 days of incubation at 20°C in 20% (w/v) PEG-3350 and 0.2 M DL-malic acid (pH 7.0). Single anomalous diffraction (SAD) data were collected to a resolution of 2.0 Å at the Zn atom absorption edge at a wavelength of 1.28 Å. The data were collected at 100 K at the beamline NW-12A of the KEK Photon Factory (Tsukuba, Japan) using HKL2000 (16), and processed by iMosflm (17). Because SAD using the anomalous signal from the single zinc atom did allow successful phasing, the structure was solved by the molecular replacement (MR) method

171 using MOLREP (18) from the CCP4 package (Collaborative Computational Project, Number 4,
172 1994). The structures of NEMO CoZi (PDB entry 3FX0) (19) and TAB2 NZF (PDB entry 2WX0)
173 (20) were used as search models for MR. One complex containing two NEMO molecules (as a
174 dimer) and one HOIP NZF1 molecule was found in each asymmetric unit of the crystal, which
175 belonged to the $P6_5$ space group. The anomalous signal from Zn atoms was used to confirm the
176 position of the Zn atom in the complex structure solved by MR. The model was further built and
177 refined using COOT (21) and REFMAC5 (22, 23). After the final refinement, NEMO CoZi amino
178 acids 252–336 and 251–337 (from the two protomers) and HOIP NZF1 amino acids 351–379 were
179 clearly visible in the electron density map. Data collection and refinement statistics are
180 summarized in Table 1. All structure figures were prepared using PyMOL (DeLano Scientific;
181 http://www.pymol.org).
182
183 ***In vitro* IKK activation assay**. Twenty-microliter samples containing 50 mM Tris-HCl (pH 7.5), 5
184 mM $MgCl_2$, 1 mM DTT, 2 mM ATP, 10 mM creatine phosphate, 50 μg/ml creatine phosphokinase,
185 phosphatase inhibitor cocktail (Nacalai Tesque), 5 μg/ml E1, 20 μg/ml UbcH5c, 10 μg/ml of
186 LUBAC, 5 μg/ml GST-IκBα (1–54); 250 μg/ml ubiquitin or 10, 50, or 250 μg/ml His_6-HA-Ub_2
187 (Fig. 1C); and 0.5, 2.5, or 5 μg/ml (Fig. 1A) or 1 μg/ml (Figs. 1B and C) IKK complex were
188 incubated for 1 h at 30°C.
189 In Figure 1B, the first ubiquitination reaction was performed in a reaction mixture containing 50

mM Tris-HCl (pH 7.5), 5 mM $MgCl_2$, 1 mM DTT, 10 mM creatine phosphate, 50 μg/ml creatine phosphokinase, 5 μg/ml E1, 20 μg/ml UbcH5c, 10 μg/ml LUBAC, and 375 μg/ml ubiquitin in the presence or absence of 2 mM ATP. The reaction ran for 90 min at 30°C; after the first reaction was stopped by addition of EDTA (10 mM) and DTT (5 mM), and the reaction mixture was incubated for 15 min at room temperature to release ubiquitin from E1, E2, and LUBAC. N-ethylmaleimide (NEM: 20 mM final concentration) was then added, and the reaction was incubated for 15 min at room temperature to inactivate E1, E2, and LUBAC, after which DTT (10 mM final concentration) was added to inactivate excess NEM. Samples were then dialyzed against buffer containing 50 mM Tris-HCl (pH 7.5) and 5 mM $MgCl_2$ to remove NEM, DTT, and EDTA. In the second-step reaction, the dialyzed mixture containing 0.2, 1, or 5 μg of ubiquitin or linear ubiquitin chains was incubated with 1 μg/ml IKK complex and 5 μg/ml GST-IκBα (1–54) in a reaction mixture containing 50 mM Tris-HCl (pH 7.5), 5 mM $MgCl_2$, 1 mM DTT, 2 mM ATP, 10 mM creatine phosphate, and 50 μg/ml creatine phosphokinase in the presence or absence of 5 μg/ml E1, 20 μg/ml UbcH5c, and 10 μg/ml LUBAC.

GST and MBP pull-down assays. Five micrograms of GST-fused WT and mutant HOIP NZF1 proteins were immobilized on glutathione-Sepharose FF beads, and then incubated for 1 h at 4°C with 1 μg of K63 diubiquitin or linear tetra-ubiquitin in buffer containing 20 mM Tris-HCl (pH 7.5), 40 μM zinc chloride, 1 mM DTT, 150 mM NaCl, and 0.1% Triton X-100. The beads were washed

three times with the same buffer.

Ten micrograms of MBP-fused WT and mutant NEMO proteins were immobilized on amylose resin, and then incubated with 1 μg of K63-diubiquitin in the presence or absence of 1 μg of GST-NZF1, 5 μg of linear tetra-ubiquitin, or 1 μg of K63-Ub_{1-7} for 1 h at 4°C in buffer containing 20 mM Tris-HCl (pH 7.5), 1 mM DTT, 150 mM NaCl, and 0.1% Triton X-100. The beads were washed three times with the same buffer, boiled in SDS sample buffer, and analyzed by immunoblotting.

***In vitro* ubiquitination assay.** Twenty-microliter samples containing 50 mM Tris-HCl (pH 7.5), 5 mM $MgCl_2$, 1 mM DTT, 2 mM ATP, 10 mM creatine phosphate, 50 μg/ml creatine phosphokinase, 5 μg/ml E1, 20 μg/ml UbcH5c, 0.5 μg/ml LUBAC, 1 μg/ml MBP-NEMO WT or Q271A/D275A, and 50 μg/ml ubiquitin were incubated at 37°C for 1 h. The reaction mixtures were subjected to immunoblotting with anti-MBP antibody.

Luciferase assays. HEK293T cells were transfected with pGL4.32 (Luc2p/NF-κB-RE/Hygro) and pGL4.74 (hRLuc/TK) (Promega), along with expression plasmids for WT or mutant HA-HOIP, Myc-HOIL-1L, and T7-SHARPIN. Twenty-four hours after transfection, cells were lysed, and luciferase activities were measured on a Lumat Luminometer (Berthold) using the Dual-Luciferase reporter assay system (Promega). N-1 cells were transfected with reporter plasmids, as described

above, along with pcDNA3.1-MMTV expression plasmid for WT or mutant NEMO. Sixteen hours after transfection, cells were stimulated with IL-1β (1 ng/ml) for 8 h, and luciferase activities were measured as described above.

***In vitro* IKK kinase assay.** NEMO-deficient MEFs stably expressing NEMO WT or Q271A/D275A were treated with TNF-α (10 ng/ml) and lysed. IKK complexes were immunoprecipitated with anti-NEMO antibody. The anti-NEMO immunoprecipitates were incubated with GST-IκBα (1–54) for 2 h at 30°C in kinase buffer (50 mM Tris-HCl [pH 7.5], 5 mM $MgCl_2$, 2 mM ATP, 10 mM creatine phosphate, 50 μg/ml creatine kinase, and phosphatase inhibitor cocktail). The reaction mixtures were subjected to immunoblotting with anti-pIκBα, anti-NEMO, and anti-GST.

TNFR1 immunoprecipitation. HOIP Δlinear MEFs retrovirally expressing HOIP WT, ΔNZF1, R369A, or T354A/F355A were treated with FH-TNF-α (3 μg/ml); cells were lysed with lysis buffer containing 10 mM Tris-HCl (pH 7.5), 150 mM NaCl, 0.2% NP-40, 10% glycerol, 2 mM PMSF, and protease inhibitor cocktail (Sigma-Aldrich), followed by centrifugation at 10,000 × *g* for 20 min at 4°C. The TNFR1 complex was immunoprecipitated by incubation with 30 μl of M2 antibody-coupled Dynabeads Protein G (Novex by Life Technologies) at 4°C for 90 min. The precipitates were washed five times with the same lysis buffer. The immunoprecipitated TNFR1

complex was eluted by incubation at 37°C for 40 min in 30 µl of TBS buffer containing 400 ng/µl 3× FLAG peptide (Sigma), and then analyzed by western blotting.

RESULTS

IKK is effectively activated by linear polyubiquitin conjugated to NEMO, but not by unanchored linear polyubiquitin.

To investigate in detail the roles of linear polyubiquitination of NEMO in IKK activation, we established an *in vitro* IKK activation assay using purified proteins. In this assay, baculovirus-purified IKK complex containing NEMO WT, or a NEMO mutant in which the critical residues for ubiquitin-binding activity were mutated to Ala (R316A/R319A/E320A in human NEMO, equivalent to R309A/R312A/E313A in mouse NEMO) (24), was incubated with GST-IκBα (1–54), E1, E2, and ubiquitin in the presence or absence of LUBAC (Fig. 1A). When incubated with the IKK complex containing NEMO WT, LUBAC generated unanchored linear chains, conjugated these linear chains to NEMO, and promoted the phosphorylation of IκBα. Phosphorylation of IκBα was also induced when a high concentration of IKK containing NEMO WT was incubated without LUBAC, possibly due to partial activation of the IKK complex during purification. However, in the presence of IKK complex containing NEMO R316A/R319A/E320A, no detectable IKK activity was induced, although generation of unconjugated linear chains was not affected by the mutation. Although the NEMO mutant was linearly ubiquitinated much more weakly than NEMO WT, we could detect linear ubiquitination when a high concentration of the NEMO mutant was incubated. These results indicated that the ubiquitin-binding activity of NEMO is involved in IKK activation, but it remains unclear why the linear ubiquitination of NEMO was

suppressed by the R316A/R319A/E320A mutation.

Both unanchored linear ubiquitin chains and linearly ubiquitinated NEMO were generated when IKK complex containing NEMO WT was activated (Fig. 1A). Therefore, to determine whether unanchored linear ubiquitin chains and/or linearly ubiquitinated NEMO are involved in IKK activation, we incubated E1, E2, LUBAC, and ubiquitin in the presence or absence of ATP, followed by treatment with DTT, EDTA, and NEM to inactivate E1, E2, and LUBAC and disassemble E1- and UbcH5c-ubiquitin (Fig. 1B). After incubation with DTT to inactivate excess NEM, and dialysis to remove NEM, DTT, and EDTA, the mixture was incubated with the IKK complex and GST-IκBα (1–54) in the presence or absence of E1, E2, and LUBAC. IκBα phosphorylation was not induced when neither unanchored nor NEMO-conjugated linear chains were generated (lanes 5–7), but efficient IκBα phosphorylation was observed in samples in which both unconjugated and NEMO-conjugated linear chains were generated in the second-step reaction (lanes 8–10). However, IκBα was not efficiently phosphorylated in samples in which unanchored linear chains, but not NEMO-conjugated linear chains, were generated in the first-step reaction (lanes 2–4). The unanchored linear chains generated in the first-step reaction appeared to be intact because they could bind the ubiquitin-binding domain of NEMO (data not shown); moreover, ubiquitin contains no Cys residues, and therefore cannot be modified by NEM. In our previous analyses, unanchored linear diubiquitin weakly activated IKK *in vitro* (15). To confirm that linear chains conjugated to NEMO activate the IKK complex much more efficiently than unanchored

linear polyubiquitin, and to determine the length of linear chains that is sufficient to activate IKK, we incubated N-terminally His_6-HA-tagged diubiquitin (His-HA-Ub_2), instead of ubiquitin monomers, in the presence or absence of E1, E2, and LUBAC (Fig. 1C). His-HA-Ub_2 can be recognized by the ubiquitin-binding domain of NEMO, and then conjugated to substrates, but cannot generate linear chains longer than diubiquitin because of its N-terminal His_6-HA tag (25). Free His-HA-Ub_2 did not overtly activate IKK (lanes 3–5), indicating that unanchored diubiquitin cannot activate IKK effectively. However, IKK was effectively activated when His-HA-Ub_2 was conjugated to NEMO by LUBAC (lanes 6–8). This result confirmed that linear chains conjugated to NEMO activate the IKK complex much more effectively than unanchored linear chains, and that conjugation of linear diubiquitin to NEMO is sufficient to activate IKK.

The HOIP NZF1 domain is involved in the recognition of NEMO by LUBAC.

Because ubiquitination often requires substrate binding by E3 enzymes (26), we hypothesized that LUBAC may also recognize NEMO prior to linear polyubiquitination of the protein. To dissect the molecular mechanism underlying linear polyubiquitination of NEMO, we probed the region of the LUBAC ligase complex that is critical for recognition of NEMO. To this end, we first expressed each subunit of LUBAC (HOIL-1L, HOIP, and SHARPIN) in HEK293T cells, with or without NEMO. Consistent with our observations in a previous study (8), HOIP co-immunoprecipitated with NEMO (Fig. 2A, lane 5). In the earlier study, deletion of the zinc finger region, containing the

zinc finger (ZF), NZF1, and NZF2 domains, attenuated the interaction between HOIP and NEMO, although HOIP Δall-ZFs could still bind to NEMO when the two proteins were co-expressed with HOIL-1L. By contrast, in this study, HOIP Δall-ZFs did not efficiently interact with NEMO even in the presence of HOIL-1L and SHARPIN (Figs. 2B and C, lane 4). The discrepancy between these observations might be attributed to the amounts of plasmids used in the transfections: in the previous study, we introduced larger amounts of the plasmids into cells than in this study.

To precisely determine the roles played by the three domains of the HOIP ZF region in the interaction with NEMO, we co-transfected WT or mutant HOIP (Fig. 2B) into HEK293T cells along with HOIL-1L, SHARPIN, and NEMO, and assessed the binding between NEMO and HOIP (Fig. 2C). Among the three domains in the zinc finger region, deletion of HOIP NZF1, but not deletion of ZF or NZF2, attenuated NEMO binding (lanes 5–7). Conversely, among HOIP mutants possessing only one of the three zinc finger domains, mutants containing NZF1, but not ZF or NZF2, could bind NEMO (lanes 8–10). These results strongly indicated that HOIP NZF1 is sufficient for the recognition of NEMO. To characterize the region of NEMO that is recognized by HOIP, we introduced NEMO mutants into HEK293T cells together with HOIL-1L, HOIP, and SHARPIN (data not shown); these experiments confirmed our previous observation (8) that NEMO lacking the CoZi region failed to bind LUBAC.

Crystal structure of NEMO CoZi in complex with HOIP NZF1.

325 To obtain further insight into the recognition of NEMO by HOIP, we determined the crystal
326 structure of the complex between the NEMO CoZi and HOIP NZF1 domains (Table 1). The crystal
327 structure contains one complex per asymmetric unit, in which NEMO and HOIP are present in 2:1
328 stoichiometry, i.e., each NEMO dimer binds one NZF1 molecule (Fig. 3A). Despite the
329 symmetrical surface on either side of NEMO, each NEMO dimer binds only one HOIP NZF1. This
330 appears to be due to crystal packing effects, because another HOIP NZF1 of a symmetry-related
331 molecule occupies the second possible binding site on NEMO. This binding mode includes weak
332 interactions between NEMO and another surface of HOIP centered on residues Thr360 and Phe361,
333 which, according to our mutational analyses, are not biologically relevant (see below, Fig. 7C).
334 However, this observation does not exclude the possibility of symmetrical binding of two HOIP
335 NZF1 molecules to NEMO in solution or *in vivo*, which might be influenced by factors such as the
336 local concentration of proteins (27). In the context of the full-length proteins, however, it seems
337 more likely that binding of a large LUBAC complex would hinder binding of a second HOIP NZF1
338 domain to a NEMO molecule. In fact, due to the transient nature of these interactions, to date we
339 have been unable to measure the stoichiometry of NEMO CoZi/HOIP NZF-1 binding using the
340 isolated domains in solution.
341 In the crystal structure, HOIP NZF1 forms a compact structure typical of NZF domains (Fig.
342 3A) (28), with a single zinc ion coordinated by four conserved cysteine residues: Cys356, Cys359,
343 Cys370, and Cys373. As shown previously, NEMO CoZi forms a coiled-coil homo-dimeric

structure (19, 24). Although NEMO CoZi bound to HOIP NZF1 retains a conformation similar to that of the free domain, the overall structures do not superimpose well, as indicated by the RMS deviation of 2.6 Å for superimposition of the Cα atoms of residues 255–335 (Fig. 3B). This structural difference appears to be due to the presence of a proline residue (Pro292) in the CoZi domain, which introduces a kink into the coiled-coil structure (24). Consistent with this explanation, the two regions N-terminal and C-terminal to Pro292 (amino acids 255–291 and 293–335, respectively) superimpose more precisely (RMS deviation of 1.1 Å and 1.3 Å, respectively) (Figs. 3C and D).

The HOIP NZF1 binding site on NEMO is located on the CC2 domain, and covers a surface area of 447.3 $Å^2$. The binding region includes amino acid residues from Gln259 to Lys270 and Glu264 to Asp275 on different protomers within the NEMO dimer (Figs. 3E and F). This surface is located at the N terminus of NEMO CoZi and does not overlap with the ubiquitin-binding domain (UBAN) (24). Thus, interaction with HOIP does not sterically hinder binding of NEMO to linear ubiquitin chains (Fig. 3A).

A hydrophobic surface on the NZF1 domain, formed by the side chains of Ala366, Val368, Leu369, Pro376, Leu378, and Ala379, serves as the major interacting partner for NEMO by contacting Ala263, Ala266, Leu267, Val268, and aliphatic portions of Gln259, Lys270, and Gln271 (Figs. 3G and H). Furthermore, Glu374, Arg375, and Arg377 from HOIP are engaged in electrostatic interactions with Lys270, Asp275, and Glu264, respectively. The Nε atom of NEMO

Gln259 forms a hydrogen bond with the main-chain carbonyl oxygen of Ala365 (Fig. 3G). Although it is not conserved among other NZF domains, the NEMO-binding surface on HOIP NZF1 is highly conserved among HOIP proteins from different species (Figs. 3I and J).

Gln271 and Asp275 of NEMO are involved in LUBAC-mediated linear polyubiquitination. Our structural analysis indicated that Gln271 and Asp275 of mouse NEMO are involved in the interaction with the HOIP NZF1 domain (Fig. 3). To confirm the importance of NEMO recognition by HOIP in linear polyubiquitination of NEMO, we generated the NEMO mutants Q271A, D275A, and Q271A/D275A and introduced them into HEK293T cells together with HOIP, HOIL-1L, and SHARPIN. Whereas NEMO WT efficiently co-immunoprecipitated with HOIP, the interactions between HOIP and the NEMO Q271A, D275A, and Q271A/D275A mutants were significantly attenuated (Fig. 4A), suggesting that Gln271 and Asp275 of NEMO are involved in recognition by HOIP *in vivo*. We also confirmed that NEMO Q271A/D275A could efficiently form the canonical IKK complex with IKK1 and IKK2 (Fig. 4B). The ubiquitin-binding activity of NEMO plays essential roles in NF-κB activation (24). Therefore, we compared the abilities of NEMO WT, Q271A, D275A, and Q271A/D275A to bind linear and Lys63-linked polyubiquitins. All three of these NEMO mutants interacted with both linear tetra-ubiquitin and Lys63-linked ubiquitin chains as efficiently as NEMO WT, which can bind both linear and Lys63 chains (longer than four ubiquitin moieties) (Figs. 4C and D) (29). These results confirmed the finding that Gln271 and

Asp275 are not located in the ubiquitin-binding domain of NEMO (Fig. 3A).

We next assessed the effect of Gln271 and/or Asp275 mutations of NEMO on its linear polyubiquitination in an *in vitro* ubiquitination assay, and found that NEMO Q271A/D275A was not efficiently ubiquitinated by LUBAC (Fig. 4E). To confirm the attenuation of linear polyubiquitination of NEMO mutants that failed to interact efficiently with HOIP in cells, we introduced NEMO WT or mutants along with the components of LUBAC into HEK293T cells, and then performed hot lysis to remove proteins non-covalently associated with NEMO (Fig. 4F). Although NEMO WT was efficiently linearly polyubiquitinated by LUBAC, linear polyubiquitination of NEMO Q271A, D275A, and Q271A/D275A was significantly attenuated.

Involvement of both linear chain conjugation to NEMO and linear chain recognition by NEMO in IKK activation.

Because the NEMO mutants (Q271A, D275A and Q271A/D275A) could not be recognized or linearly polyubiquitinated by LUBAC, but could form IKK complexes with IKK1 and IKK2 and bind to ubiquitin chains as well as NEMO WT, they appeared to be suitable tools for probing the roles of linear polyubiquitination of NEMO in signal-induced NF-κB activation. We therefore transiently introduced NEMO WT or mutants, together with the 5× NF-κB luciferase reporter, into a NEMO-deficient subclone (N-1) of the Rat-1 fibroblast line. Luciferase assays revealed that the Q271A, D275A, and Q271A/D275A mutations of NEMO attenuated IL-β-induced NF-κB

activation (Fig. 5A, upper). The introduced NEMO WT and mutant proteins were expressed at almost identical levels (Fig. 5A, lower) that were slightly lower than the level of endogenous NEMO expression in the parental Rat-1 cells (data not shown). When NEMO WT or Q271A/D275A was retrovirally introduced into the NEMO-defective N-1 cells, IL-1β-induced linear polyubiquitination and IκBα phosphorylation were significantly attenuated by Q271A/D275A mutation (Fig. 5B). We also stably introduced NEMO WT or Q271A/D275A into the NEMO-deficient MEFs; these proteins were expressed at levels comparable to, or slightly lower than, that of endogenous NEMO in WT MEFs (data not shown). In the NEMO-deficient MEFs complemented with NEMO WT, treatment with TNF-α induced phosphorylation and degradation of IκBα (Fig. 5C). By contrast, in cells expressing NEMO Q271A/D275A, TNF-α-mediated phosphorylation and degradation of IκBα were significantly attenuated (Fig. 5C). Furthermore, TNF-α induced the IKK activity in anti-NEMO immunoprecipitates from cells expressing NEMO WT, whereas TNF-α did not overtly induce IKK activity in NEMO Q271A/D275A-expressing cells (Fig. 5D).

Lys278 and Lys302 of mouse NEMO, which are equivalent to Lys285 and Lys309 of human NEMO, are major sites of linear polyubiquitination by LUBAC (8). The UBAN motif, the major ubiquitin-binding site of NEMO, preferentially binds to linear diubiquitin relative to Lys63-linked diubiquitin. Within this motif, Phe305 is involved in the binding of both linear and Lys63-linked diubiquitin, whereas Glu313 is specifically involved in linear diubiquitin recognition

(24). To investigate the functional interaction between HOIP binding and linear polyubiquitination of, or recognition of linear ubiquitin chains by, NEMO, we transiently expressed the NEMO mutants indicated in Figure 6A in N-1 cells and assessed IL-1β-induced NF-κB activation by luciferase assays. The introduced NEMO WT and mutants were expressed at almost identical levels (Fig. 6A) that were slightly lower than the endogenous NEMO expression level in the parental Rat-1 cells (data not shown). Introduction of mutations at the major polyubiquitination sites, K278R/K302R (QDKK/AARR), into NEMO Q271A/D275A failed to further suppress IL-1β-induced NF-κB activation attenuated by Q271A/D275A mutation, thus confirming that the NEMO recognition by NZF1 of HOIP attenuates LUBAC-induced linear polyubiquitination of the protein. Mutation of Glu313 to Ala (NEMO E313A) marginally suppresses NF-κB activation by partially impairing linear chain binding (24), an observation confirmed in this study (Fig. 6A). To investigate whether impaired recognition of linear ubiquitin chains and NEMO would additively suppress IL-1β-induced NF-κB activation, we generated NEMO Q271A/D275A/E313A (QD/AA/E313A). This triple mutant attenuated IL-1β-induced NF-κB activation to a greater extent than NEMO Q271A/D275A or NEMO E313A. However, the NEMO F305A mutant, which abolishes NEMO binding to both linear and Lys63-linked chains almost completely (24), strongly suppressed IL-1β-induced NF-κB activation, confirming the importance of ubiquitin binding by NEMO for NF-κB activation. These results suggested that conjugation of linear chains to NEMO, and recognition of linear ubiquitin chains by NEMO, are synergistically involved in signal-induced

NF-κB activation.

IKK2, a crucial kinase within the IKK complex that phosphorylates IκBα, homodimerizes via its kinase domain (KD), leading to activation of IKK via *trans* auto-phosphorylation (30). We examined the involvement of KD homodimerization of IKK2 in the activation of IKK provoked by linearly ubiquitinated NEMO. Val229, His232, Tyr294, Gly295, and Pro296 of human IKK2 are involved in the KD-KD interaction of IKK2 (30). Therefore, we mutated Val229 and His232 to Ala (V229A/H232A); in another construct, Tyr294, Gly295, and Pro296 were mutated to Leu, Lys, and Gln, respectively, the corresponding amino acids in IKK1 (Y294L/G295K/P296Q) (30). IKK becomes constitutively active when Ser177 and Ser181 in the activation loop of IKK2 are mutated to phosphomimetic Glu (S177E/S181E) (30). IKK2 V229A/Y232A and Y294L/G295K/P296Q with the S177E/S181E mutations can effectively phosphorylate IκBα (30), suggesting that both of these IKK2 mutants can function as a kinase when specific Ser residues are phosphorylated. NEMO-Ub_2, a NEMO mutant with uncleavable linear di-ubiquitin at the C-terminus, mimics linearly ubiquitinated NEMO, and the introduction of NEMO-Ub_2 alone to HEK293T cells induces IKK activation (15). With these observations in mind, we evaluated mutations of IKK2 that abolish the KD-KD interaction upon NEMO-Ub_2-mediated activation of IKK. Because IKK2 can be activated even when transiently introduced alone (30), we introduced smaller amounts of IKK2 plasmids into HEK293T cells than in previous reports. As expected, under these assay conditions, IKK2 WT or mutants were not activated when IKK2 was introduced alone (Fig. 6B). When

introduced together with NEMO, IKK2 WT was weakly phosphorylated in its activation loop; because IKK2 in NEMO-deficient cells is not effectively activated (31), this phosphorylation may have been due to an IKK2-NEMO interaction. We have observed that NEMO-Ub_2 induces phosphorylation of IKK2 WT much more efficiently than NEMO. However, NEMO-Ub_2 failed to induce phosphorylation of IKK2 V229A/Y232A or Y294L/G295K/P296Q, indicating that the KD-KD interaction is necessary for the activation of IKK2 by NEMO-Ub_2. Because IKK2 V229A/Y232A and Y294L/G295K/P296Q could form complexes with NEMO and NEMO-Ub_2, as well as IKK2 WT (Fig. 6C), these observations indicate that recognition of the linear chain conjugated to NEMO, possibly by another NEMO molecule, plays crucial roles in IKK activation and subsequent NF-κB activation by inducing *trans* auto-phosphorylation of IKK2.

The NEMO- and ubiquitin-binding activities of HOIP NZF1 are both involved in NF-κB activation by LUBAC.

Our crystallographic analyses revealed that HOIP NZF1 is involved in NEMO recognition, and that Arg369 in the NZF1 domain of mouse HOIP (equivalent to Arg375 in human HOIP, used for the crystallographic analyses described above) contributes significantly to interaction with NEMO (Fig. 3G). However, NZF domains are classified as potential ubiquitin-binding modules (28, 32) and HOIP NZF1 has also been reported to bind ubiquitin (11). The highly conserved TF/Φ motif of NZF domains (Φ indicates a hydrophobic residue that is separated from TF (Thr-Phe) by ten

residues (33)), is crucial for the ubiquitin-binding activity (33). Because Thr354 and Phe355 of TF/Φ motif in mouse HOIP NZF1 (equivalent to Thr360 and Phe361 in human HOIP) are highly conserved (Fig. 3J), it is reasonable to speculate that HOIP NZF1 might exhibit the ubiquitin-binding activity as well as NEMO-binding activity. To confirm the ability of NZF1 to bind ubiquitin, we generated the mouse HOIP NZF1 mutants R369A, T354A, F355A, and T354A/F355A. GST pull-down assays revealed that the T354A, F355A, and T354A/F355A mutations, but not R369A, attenuated binding of HOIP NZF1 to not only Lys63-linked diubiquitin but also linear tetra-ubiquitin (Figs. 7A and B). To investigate the effect of T354A, F355A, and T354A/F355A mutations on NEMO binding, we co-transfected HOIP WT or mutants into HEK293T cells along with HOIL-1L, SHARPIN, and NEMO. HOIP WT, T354A, F355A, and T354A/F355A efficiently co-immunoprecipitated with NEMO, whereas HOIP ΔNZF1 and R369A mutants failed to interact with NEMO (Fig. 7C). From these results, we draw the following conclusions: NZF1 can bind to both ubiquitin and NEMO; Arg369 of HOIP NZF1 is involved in NEMO recognition but not ubiquitin binding; and T354 and F355 are involved in ubiquitin recognition but not NEMO binding. Furthermore, the *in vitro* binding assay using purified proteins revealed that NZF1 and Lys63-linked diubiquitin were both pulled down with MBP-NEMO, indicating that NZF1 bound simultaneously to Lys63-linked diubiquitin and NEMO (Fig. 7D).

To probe the roles of the ubiquitin- and NEMO-binding activities of NZF1 of HOIP in LUBAC-mediated NF-κB activation, we used luciferase assays to evaluate NF-κB activation

mediated by exogenously introduced LUBAC. LUBAC-mediated NF-κB activation was suppressed in HEK293T cells transfected with HOIP R369A or HOIP ΔNZF1. Introduction of HOIP T354A/F355A also suppressed LUBAC-mediated NF-κB activation, but the suppression was significantly weaker than that mediated by HOIP R369A (Fig. 7E). To further examine the roles of the ubiquitin- and NEMO-binding activities of HOIP NZF1 in TNF-α-mediated NF-κB activation, we introduced WT or HOIP mutants into HOIP Δlinear MEFs; the HOIP mutants were expressed at levels identical to or a little higher than that of HOIP WT (data not shown). In cells expressing HOIP R369A or T354A/F355A, IκBα degradation was slower than in HOIP WT-expressing cells; the extent of the delay in these two mutants was similar to that expressing HOIP ΔNZF1 (Figs. 7F and G). The ubiquitin-binding activity of HOIP has been implicated in the recruitment of LUBAC to the activated TNF-R1 signaling complex (TNF-RSC) (34). ΔNZF and T354A/F355A mutations of HOIP attenuated TNF-α-induced recruitment of HOIP to TNF-RSC, but the R369A mutation did not overtly suppress HOIP recruitment to the activated receptor complex (Fig. 7H). Importantly, HOIP WT and R369A mutant were recruited to TNF-RSC at similar levels, but ubiquitination of NEMO was significantly abrogated by the R369A mutation.

These results strongly indicated that NZF1 of HOIP can simultaneously bind both NEMO and ubiquitin, and that both interactions are involved in TNF-α-mediated NF-κB activation. Loss of NEMO binding impairs linear polyubiquitination of NEMO, whereas loss of ubiquitin binding impairs recruitment of LUBAC to TNF-RSC. However, loss of NEMO binding by HOIP NZF1

appears to exert a more profound effect on LUBAC-mediated NF-κB activation than loss of ubiquitin binding. Although the interaction between HOIP NZF1 and NEMO was abolished almost completely by the mutations described above, neither TNF-α- nor LUBAC-mediated NF-κB activation was completely suppressed in cells expressing these mutants. We propose mechanisms that might underlie this residual NF-κB activation in the Discussion section.

DISCUSSION

In this study, we showed that recognition of linear ubiquitin chains by NEMO and conjugation of those chains to NEMO are synergistically involved in IKK activation. The IKK complex is activated by phosphorylation of the IKK2 subunit (35). In general, phosphorylation of kinases is mediated either by *trans* auto-phosphorylation or by upstream kinases (36). The crystal structure of *Xenopus* IKK2, determined recently, reveals that IKK2 contains a dimerization domain (31); dimerization-defective IKK2 mutants fail to be activated. Furthermore, analysis of the crystal structure of human IKK2 revealed that homotypic interaction of the IKK2 KD is crucial for IKK2 activation (30). We also showed here that IKK2 mutants that are defective in KD-KD interaction could not be activated by NEMO-Ub_2, which mimics linearly ubiquitinated NEMO. These results strongly indicate that IKK2 activation mediated by linear chains requires *trans* auto-phosphorylation; thus it seems plausible that linear chains conjugated to NEMO by LUBAC are recognized by NEMO *in trans* on another IKK complex, thereby inducing multimerization of IKK complexes. Upon multimerization, IKK2 could dimerize and *trans* auto-phosphorylate (Fig. 8). It is possible that binding of ubiquitin to the UBAN domain induces conformational changes in NEMO, thereby changing the positions of IKK1 and IKK2, leading to phosphorylation of IKK2. However, considering the results of structural analyses of IKK2, together with our observations, the former scenario seems more likely (37).

We have probed the interactions between HOIP and NEMO by solving a co-crystal structure of NZF1 of human HOIP and CoZi of mouse NEMO while our mutational studies have been performed using mouse HOIP. However, the surface residues from HOIP that interact with NEMO are fully conserved in human and mouse species (Fig. 3J). Our mutational analyses based on the structure of the co-crystal show that direct recognition of NEMO by HOIP plays a major role in NF-κB activation following conjugation of linear chains to NEMO. Although the RING-IBR-RING region of HOIP is the catalytic center for linear polyubiquitination by LUBAC (7), recent results obtained using an *in vitro* ubiquitin assay have suggested that the RING2 domain of HOIL-1L plays a role in linear polyubiquitination of NEMO (38). However, given that the HOIP-SHARPIN complex effectively linearly polyubiquitinates NEMO *in vitro* and activates NF-κB in cells (12), any involvement of the RING2 domain of HOIL-1L in linear polyubiquitination of NEMO and NF-κB activation seems likely to be marginal. Thus, HOIP plays central roles in LUBAC-mediated NF-κB activation via direct recognition of linear polyubiquitin and conjugation of this molecule to NEMO. However, neither NF-κB activation nor linear polyubiquitination of NEMO was completely abolished in NEMO Q271A/D275A, which evades recognition by LUBAC. We suspect that the residual activation might be caused by the presence of one or more additional NEMO recognition sites. Consistent with this idea, the NEMO-LUBAC interaction cannot be completely abolished by mutations in HOIP NZF1, although HOIP NZF1 does appear to be the primary NEMO recognition site. In support of this possibility, in our previous

558 report (8), we observed that HOIP lacking NZF1 could bind NEMO in the presence of high levels
559 of HOIL-1L. Alternatively, in light of observations that the linear polyubiquitination activity of
560 LUBAC is dispensable for NF-κB activation via B-cell antigen receptor (39), residual NF-κB
561 activation might be mediated by other IKK activation pathways. The kinase TAK1 has been
562 suggested to activate IKK2 (40); specifically, TAK1-mediated IKK activation has been proposed to
563 involve the Lys63 chain-binding activity of TAB2 and TAB3, which form a complex with TAK1
564 (41). Recently, Lys63 and linear hybrid chains have been implicated in IKK activation (42). It is
565 hypothesized that both the TAK1 and IKK complexes bind simultaneously to one hybrid chain
566 composed of Lys63 and linear linkages, generated upon IL-1β stimulation, thereby inducing
567 phosphorylation of IKK2 (42). In addition to the UBAN motif that preferentially binds linear
568 chains, NEMO possesses another ubiquitin-binding domain, the ZF domain, in its C-terminus.
569 NEMO can bind longer Lys63-linked chains by utilizing both the UBAN and ZF domains,
570 potentially inducing IKK activation by multimerizing the IKK complex. Because the
571 NEMO-LUBAC interaction appears dispensable for the generation of the Lys63 and Lys63/linear
572 hybrid chains, the residual NF-κB activation in NEMO Q271A/D275A-expressing cells might be
573 attributed to these ubiquitin chains, as distinct from linear chains. However, considering our results
574 described here, together with the previous observation that Lys63-linked chains are dispensable for
575 TNF-α-mediated NF-κB activation (43), it seems likely that linear chain-mediated *trans*
576 auto-phosphorylation of IKK2 plays a major role in NF-κB activation, at least in the case of

activation mediated by the TNF receptor family. In further support of this notion, we observed previously that CD40-mediated NF-κB activation is almost completely abolished in B-cells from mice lacking the linear polyubiquitination activity of LUBAC (39). Further dissection of the mechanism underlying IKK activation via LUBAC-mediated linear polyubiquitination will be needed to clarify the involvement of linear chain-mediated dimerization of IKK2 in NF-κB activation induced by various stimuli, including IL-1β.

We also showed here that HOIP NZF1 simultaneously binds NEMO and ubiquitin (Fig. 7D). The TF/Φ motifs of the HOIP NZF domains, which are crucial for ubiquitin binding by NZFs, are highly conserved. Consistent with this, the T354A, F355A, and T354A/F355A mutants of HOIP NZF1 failed to bind ubiquitin. By contrast, NZF1 R369A could bind ubiquitin as efficiently as WT NZF1 (Figs. 7A and B). Recruitment of LUBAC to TNF-RSC upon TNF-α stimulation is a prerequisite for TNF-α-mediated NF-κB activation, and the ubiquitin-binding activity of LUBAC is required for this recruitment (34). We observed in this study that the T354A/F355A double mutation, but not the R369A mutation, of HOIP attenuated TNF-α-induced recruitment of HOIP to TNF-RSC (Fig. 7H). Furthermore, we observed that both HOIP R369A and T354A/F355A attenuated TNF-α-induced NF-κB activation at a level comparable to that of HOIP ΔNZF1 when expressed in HOIP Δlinear MEFs (Figs. 7F and G). However, the luciferase assays revealed that HOIP R369A, but not T354A, F355A, or T354A/F355A, significantly suppressed NF-κB activation induced by the introduction of LUBAC components (Fig. 7E). Recruitment of LUBAC

596 to TNF-RSC is a prerequisite for TNF-α-mediated NF-κB activation, but is apparently not required
597 for NF-κB activation provoked by the exogenous introduction of LUBAC components; this may
598 explain why the R369A mutation of HOIP suppressed LUBAC-mediated NF-κB activation more
599 severely than the T354A/F355A mutation.

600 In summary, we dissected the roles of linear polyubiquitination in NF-κB activation and
601 showed that recognition of linear polyubiquitin conjugated to NEMO, possibly by NEMO in
602 another IKK complex, induces *trans* auto-phosphorylation of IKK2 and subsequent activation of
603 NF-κB. The NZF1 domain of HOIP is involved in the linear polyubiquitination of NEMO by
604 recognizing NEMO, leading to the homo-dimerization of IKK2. In addition to NEMO recognition,
605 HOIP NZF1 plays another role in signal-induced NF-κB activation: the recruitment of LUBAC to
606 the activated receptor complexes via its ubiquitin-binding activity (Fig. 8). Amino acid residues
607 crucial for ubiquitin binding are conserved in HOIP NZF1 (Fig. 3I), whereas other residues are not
608 conserved in other human NZFs. By contrast, the NEMO-binding surface on HOIP NZF1 is highly
609 conserved in NZF1s of vertebrate HOIP proteins (Fig. 3J). Because HOIP NZF1 can bind to both
610 ubiquitin and NEMO simultaneously (Fig. 7D), we conclude that HOIP NZF1 plays a critical role
611 in signal-induced activation by recruiting LUBAC to the site of function and ubiquitinating
612 substrate to activate NF-κB on site.
613

Accession code. Atomic coordinates and structure factors of the NEMO CoZi/HOIP NZF1 complex structure have been deposited in the Protein Data Bank under accession code 4O4M.

ACKNOWLEDGEMENTS

We thank Dr. T. Kitamura, Dr. R. Baker, and Dr. H. Kamata for providing pMX-IP, USP2cc, and NEMO-deficient MEFs, respectively. This work was partly supported by the Targeted Proteins Research Program (TPRP) and grants from the Ministry of Education, Culture, Sports, Science, and Technology of Japan to K.I. and S.W.. S.R. was a recipient of the JSPS Invitation Fellowship for Research in Japan (Long-term).

REFERENCES

1. **Vallabhapurapu S, Karin M.** 2009. Regulation and function of NF-κB transcription factors in the immune system. Annu. Rev. Immunol. **27:**693-733.
2. **Karin M.** 2006. Nuclear factor-κB in cancer development and progression. Nature **441:**431-436.
3. **Li Q, Verma IM.** 2002. NF-κB regulation in the immune system. Nat. Rev. Immunol. **2:**725-734.
4. **Baltimore D.** 2011. NF-κB is 25. Nat. Immunol. **12:**683-685.
5. **Hayden MS, Ghosh S.** 2008. Shared principles in NF-κB signaling. Cell **132:**344-362.
6. **Skaug B, Jiang X, Chen ZJ.** 2009. The role of ubiquitin in NF-κB regulatory pathways. Annual. Rev. Biochem. **78:**769-796.
7. **Kirisako T, Kamei K, Murata S, Kato M, Fukumoto H, Kanie M, Sano S, Tokunaga F, Tanaka K, Iwai K.** 2006. A ubiquitin ligase complex assembles linear polyubiquitin chains. EMBO J. **25:**4877-4887.
8. **Tokunaga F, Sakata S, Saeki Y, Satomi Y, Kirisako T, Kamei K, Nakagawa T, Kato M, Murata S, Yamaoka S, Yamamoto M, Akira S, Takao T, Tanaka K, Iwai K.** 2009. Involvement of linear polyubiquitylation of NEMO in NF-κB activation. Nat. Cell Biol. **11:**123-132.
9. **Boisson B, Laplantine E, Prando C, Giliani S, Israelsson E, Xu Z, Abhyankar A,**

Israel L, Trevejo-Nunez G, Bogunovic D, Cepika AM, MacDuff D, Chrabieh M, Hubeau M, Bajolle F, Debre M, Mazzolari E, Vairo D, Agou F, Virgin HW, Bossuyt X, Rambaud C, Facchetti F, Bonnet D, Quartier P, Fournet JC, Pascual V, Chaussabel D, Notarangelo LD, Puel A, Israel A, Casanova JL, Picard C. 2012. Immunodeficiency, autoinflammation and amylopectinosis in humans with inherited HOIL-1 and LUBAC deficiency. Nat. Immunol. **13:**1178-1186.

10. **Gerlach B, Cordier SM, Schmukle AC, Emmerich CH, Rieser E, Haas TL, Webb AI, Rickard JA, Anderton H, Wong WW, Nachbur U, Gangoda L, Warnken U, Purcell AW, Silke J, Walczak H.** 2011. Linear ubiquitination prevents inflammation and regulates immune signalling. Nature **471:**591-596.

11. **Ikeda F, Deribe YL, Skanland SS, Stieglitz B, Grabbe C, Franz-Wachtel M, van Wijk SJ, Goswami P, Nagy V, Terzic J, Tokunaga F, Androulidaki A, Nakagawa T, Pasparakis M, Iwai K, Sundberg JP, Schaefer L, Rittinger K, Macek B, Dikic I.** 2011. SHARPIN forms a linear ubiquitin ligase complex regulating NF-κB activity and apoptosis. Nature **471:**637-641.

12. **Tokunaga F, Nakagawa T, Nakahara M, Saeki Y, Taniguchi M, Sakata S, Tanaka K, Nakano H, Iwai K.** 2011. SHARPIN is a component of the NF-κB-activating linear ubiquitin chain assembly complex. Nature **471:**633-636.

13. **Saito N, Courtois G, Chiba A, Yamamoto N, Nitta T, Hironaka N, Rowe M, Yamaoka**

S. 2003. Two carboxyl-terminal activation regions of Epstein-Barr virus latent membrane protein 1 activate NF-κB through distinct signaling pathways in fibroblast cell lines. J. Biol. Chem. **278:**46565-46575.

14. **Catanzariti AM, Soboleva TA, Jans DA, Board PG, Baker RT.** 2004. An efficient system for high-level expression and easy purification of authentic recombinant proteins. Protein Sci. **13:**1331-1339.

15. **Kensche T, Tokunaga F, Ikeda F, Goto E, Iwai K, Dikic I.** 2012. Analysis of nuclear factor-κB (NF-κB) essential modulator (NEMO) binding to linear and lysine-linked ubiquitin chains and its role in the activation of NF-κB. J. Biol. Chem. **287:**23626-23634.

16. **Otwinowski Z, Minor W.** 1997. Processing of X-ray diffraction data collected in oscillation mode. Methods Enzymol. **276:**307-326.

17. **Leslie AW, Powell H.** 2007. Processing diffraction data with mosflm. Evolving Methods for Macromolecular Crystallography. **245:**41-51

18. **Vagin A, Teplyakov A.** 1997. MOLREP: an Automated Program for Molecular Replacement. J. Appl. Cryst. **30:**1022-1025.

19. **Lo YC, Lin SC, Rospigliosi CC, Conze DB, Wu CJ, Ashwell JD, Eliezer D, Wu H.** 2009. Structural basis for recognition of diubiquitins by NEMO. Mol. Cell **33:**602-615.

20. **Sato Y, Yoshikawa A, Yamashita M, Yamagata A, Fukai S.** 2009. Structural basis for specific recognition of Lys 63-linked polyubiquitin chains by NZF domains of TAB2 and

TAB3. EMBO J. **28:**3903-3909.

21. **Emsley P, Cowtan K.** 2004. Coot: model-building tools for molecular graphics. Acta Crystallogr. D, Biol. Cryst. **60:**2126-2132.

22. **Murshudov GN, Skubak P, Lebedev AA, Pannu NS, Steiner RA, Nicholls RA, Winn MD, Long F, Vagin AA.** 2011. REFMAC5 for the refinement of macromolecular crystal structures. Acta Crystallogr. D, Biol. Cryst. **67:**355-367.

23. **Murshudov GN, Vagin AA, Dodson EJ.** 1997. Refinement of macromolecular structures by the maximum-likelihood method. Acta Crystallogr. D, Biol. Cryst. **53:**240-255.

24. **Rahighi S, Ikeda F, Kawasaki M, Akutsu M, Suzuki N, Kato R, Kensche T, Uejima T, Bloor S, Komander D, Randow F, Wakatsuki S, Dikic I.** 2009. Specific recognition of linear ubiquitin chains by NEMO is important for NF-κB activation. Cell **136:**1098-1109.

25. **Smit JJ, Monteferrario D, Noordermeer SM, van Dijk WJ, van der Reijden BA, Sixma TK.** 2012. The E3 ligase HOIP specifies linear ubiquitin chain assembly through its RING-IBR-RING domain and the unique LDD extension. EMBO J. **31:**3833-3844.

26. **Jackson PK, Eldridge AG, Freed E, Furstenthal L, Hsu JY, Kaiser BK, Reimann JD.** 2000. The lore of the RINGs: substrate recognition and catalysis by ubiquitin ligases. Trends Cell Biol. **10:**429-439.

27. **Ivins FJ, Montgomery MG, Smith SJ, Morris-Davies AC, Taylor IA, Rittinger K.** 2009. NEMO oligomerization and its ubiquitin-binding properties. The Biochemical

journal **421:**243-251.

28. **Wang B, Alam SL, Meyer HH, Payne M, Stemmler TL, Davis DR, Sundquist WI.** 2003. Structure and ubiquitin interactions of the conserved zinc finger domain of Npl4. J. Biol. Chem. **278:**20225-20234.

29. **Laplantine E, Fontan E, Chiaravalli J, Lopez T, Lakisic G, Veron M, Agou F, Israel A.** 2009. NEMO specifically recognizes K63-linked poly-ubiquitin chains through a new bipartite ubiquitin-binding domain. EMBO J. **28:**2885-2895.

30. **Polley S, Huang DB, Hauenstein AV, Fusco AJ, Zhong X, Vu D, Schrofelbauer B, Kim Y, Hoffmann A, Verma IM, Ghosh G, Huxford T.** 2013. A Structural Basis for IκB Kinase 2 Activation Via Oligomerization-Dependent Trans Auto-Phosphorylation. PLoS Biol. **11:**e1001581.

31. **Xu G, Lo YC, Li Q, Napolitano G, Wu X, Jiang X, Dreano M, Karin M, Wu H.** 2011. Crystal structure of inhibitor of κB kinase β. Nature **472:**325-330.

32. **Meyer HH, Wang Y, Warren G.** 2002. Direct binding of ubiquitin conjugates by the mammalian p97 adaptor complexes, p47 and Ufd1-Npl4. EMBO J. **21:**5645-5652.

33. **Alam SL, Sun J, Payne M, Welch BD, Blake BK, Davis DR, Meyer HH, Emr SD, Sundquist WI.** 2004. Ubiquitin interactions of NZF zinc fingers. EMBO J. **23:**1411-1421.

34. **Haas TL, Emmerich CH, Gerlach B, Schmukle AC, Cordier SM, Rieser E, Feltham R, Vince J, Warnken U, Wenger T, Koschny R, Komander D, Silke J, Walczak H.** 2009.

Recruitment of the linear ubiquitin chain assembly complex stabilizes the TNF-R1 signaling complex and is required for TNF-mediated gene induction. Mol. Cell **36:**831-844.

35. **Israel A.** 2010. The IKK complex, a central regulator of NF-κB activation. Cold Spring Harbor perspectives in biology **2:**a000158.

36. **Hunter T, Lindberg RA, Middlemas DS, Tracy S, van der Geer P.** 1992. Receptor protein tyrosine kinases and phosphatases. Cold Spring Harbor symposia on quantitative biology **57:**25-41.

37. **Iwai K.** 2012. Diverse ubiquitin signaling in NF-κB activation. Trends Cell Biol. **22:**355-364.

38. **Smit JJ, van Dijk WJ, El Atmioui D, Merkx R, Ovaa H, Sixma TK.** 2013. Target Specificity of the E3 Ligase LUBAC for Ubiquitin and NEMO Relies on Different Minimal Requirements. J. Biol. Chem. **288:**31728-31737.

39. **Sasaki Y, Sano S, Nakahara M, Murata S, Kometani K, Aiba Y, Sakamoto S, Watanabe Y, Tanaka K, Kurosaki T, Iwai K.** 2013. Defective immune responses in mice lacking LUBAC-mediated linear ubiquitination in B cells. EMBO J. **32:**2463-2476.

40. **Wang C, Deng L, Hong M, Akkaraju GR, Inoue J, Chen ZJ.** 2001. TAK1 is a ubiquitin-dependent kinase of MKK and IKK. Nature **412:**346-351.

41. **Kanayama A, Seth RB, Sun L, Ea CK, Hong M, Shaito A, Chiu YH, Deng L, Chen ZJ.**

2004. TAB2 and TAB3 activate the NF-κB pathway through binding to polyubiquitin chains. Mol. Cell **15:**535-548.

42. **Emmerich CH, Ordureau A, Strickson S, Arthur JS, Pedrioli PG, Komander D, Cohen P.** 2013. Activation of the canonical IKK complex by K63/M1-linked hybrid ubiquitin chains. Proc. Natl. Acad. Sci. USA **110:**15247-15252.

43. **Xu M, Skaug B, Zeng W, Chen ZJ.** 2009. A ubiquitin replacement strategy in human cells reveals distinct mechanisms of IKK activation by TNFα and IL-1β. Mol. Cell **36:**302-314.

749 **FIGURE LEGENDS**

750

751 **FIGURE 1.** Linearly ubiquitinated NEMO activates the IKK complex more efficiently than
752 unanchored linear ubiquitin chains. (A) IKK complex (0.5, 2.5 or 5 μg/ml) and either NEMO WT
753 or R316A/R319A/E320A was incubated for 1 h at 30°C with GST-IκBα (1–54), E1, and UbcH5c
754 in the presence or absence of LUBAC, and the reaction mixtures were probed with the indicated
755 antibodies. (B) Reaction mixtures containing E1, E2, LUBAC, and ubiquitin were incubated with
756 or without ATP. After incubation, E1, E2, and LUBAC were inactivated with EDTA and NEM, and
757 the reaction mixtures were dialyzed. The dialyzed samples were incubated with GST-IκBα (1–54)
758 and the IKK complex in the presence or absence of E1, E2, and LUBAC, followed by probing with
759 the indicated antibodies. (C) His-HA-Ub_2 (10, 50, or 250 μg/ml) or 250 μg/ml ubiquitin was
760 incubated with E1, UbcH5c, LUBAC, IKK complex, and GST-IκBα (1–54), followed by probing
761 with the indicated antibodies.

762

763 **FIGURE 2.** The NZF1 domain of HOIP is responsible for NEMO binding. (A) Myc-HOIP,
764 Myc-HOIL-1L, or Myc-SHARPIN were transfected into HEK293T cells with or without
765 FLAG-NEMO, and cell lysates and anti-FLAG immunoprecipitates were immunoblotted with the
766 indicated antibodies. (B) Schematics of HOIP and its mutants. (C) HA-HOIP and its mutants, along
767 with Myc-HOIL-1L, T7-SHARPIN, and FLAG-NEMO, were transfected into HEK293T cells.

768 Cell lysates (top) and anti-HA immunoprecipitates (bottom) were immunoblotted with the
769 indicated antibodies.
770
771 **FIGURE 3.** Structure of the NEMO CoZi in complex with HOIP NZF1. (A) Overall structure of
772 the NEMO CoZi/HOIP NZF1 complex. The two chains of NEMO are colored in yellow and green;
773 HOIP is shown in salmon. The coiled-coil2 and LZ (CoZi) and UBAN (ubiquitin-binding in ABIN
774 proteins and NEMO) domains are indicated on the NEMO structure. (B to D) Superposition of the
775 NEMO molecules in the free form (light orange) and in complex with HOIP NZF1 (green),
776 including residues (B) 255–335, (C) 255–291, and (D) 293–335. Arrows indicate position of the
777 Pro292 residues in the NEMO structure. (E and F) Amino acid residues involved in the interactions
778 are indicated on the surfaces of NEMO (E) and HOIP (F). (G) Stereo view of the interactions
779 between NEMO CoZi and HOIP NZF1. Interacting amino acids are shown as sticks. Salt bridges
780 and hydrogen bonds are indicated with dashed lines. (H) Open-book representation of NEMO
781 recognition by HOIP NZF1. (I) Analysis of conservation of residues of HOIP NZF1 involved in
782 binding to NEMO in different NZF domain-containing proteins. Interacting residues from HOIP
783 NZF1 and conserved residues are highlighted in red. (J) Analysis of conservation of residues of
784 HOIP NZF1 involved in binding to NEMO in various species. Highly conserved residues are
785 highlighted in dark gray, and less conserved residues in light gray. The red arrows indicate residues
786 from human HOIP that interact with NEMO.

787

788 **FIGURE 4.** Involvement of Gln271 and Asp275 of NEMO in LUBAC-mediated linear
789 polyubiquitination. (A) HEK293T cells were transfected as indicated, and cell lysates (top),
790 anti-FLAG immunoprecipitates (middle), and anti-HA immunoprecipitates (bottom) were
791 immunoblotted. (B) HEK293T cells were transfected as indicated, and cell lysates (bottom) and
792 anti-FLAG immunoprecipitates (top) were immunoblotted. (C and D) NEMO WT or mutants
793 fused with MBP were incubated with linear tetra-ubiquitin (C) or K63 chains (D) followed by
794 pull-down with maltose resins. (E) MBP-NEMO WT or Q271A/D275A was incubated as indicated
795 at 37°C for 1 h, followed by immunoblotting with anti-MBP antibody. (F) FLAG-NEMO or its
796 mutants were introduced into HEK293T cells together with LUBAC. Cells were subjected to hot
797 lysis, and anti-FLAG immunoprecipitates were probed with anti-linear ubiquitin or anti-FLAG
798 antibody.

799

800 **FIGURE 5.** Conjugation of linear chains to NEMO plays crucial roles in IKK activation. (A)
801 NEMO-defective N-1 cells were transiently transfected with 5× NF-κB luciferase reporter and
802 NEMO WT or mutants. At 16 h after transfection, cells were treated with IL-1β (1 ng/ml) for 8 h,
803 and luciferase activity was measured (mean ± SEM; n=3). The amounts of NEMO and tubulin
804 were also assessed. (B) N-1 cells expressing NEMO WT or Q271A/D275A were treated with
805 IL-1β (20 ng/ml) for the indicated periods, and anti-NEMO immunoprecipitates were

immunoblotted. (C) NEMO-deficient MEFs stably expressing NEMO WT or Q271A/D275A were treated with TNF-α (10 ng/ml) for the indicated periods, and cell lysates were immunoblotted with the indicated antibodies. (D) Anti-NEMO immunoprecipitates from NEMO-deficient MEFs stably expressing NEMO WT or Q271A/D275A treated with TNF-α (10 ng/ml) for the indicated periods were incubated with GST-IκBα (1–54) at 30°C for 2 h. The reaction mixtures were probed with the indicated antibodies.

FIGURE 6. Mechanism underlying IKK activation mediated by LUBAC. (A) NEMO-defective N-1 cells were transiently transfected with 5× NF-κB luciferase reporter and NEMO WT or mutants. At 16 h after transfection, cells were treated with IL-1β (1 ng/ml) for 8 h, and luciferase activity was measured (mean ± SEM n=3). The amounts of NEMO and tubulin were also assessed. (B) FLAG-IKK2 or its mutants, along with FLAG-NEMO or FLAG-NEMO-Ub_2, were transfected into HEK293T cells; cell lysates were immunoblotted with the indicated antibodies. (C) FLAG-IKK2 and its mutants, along with FLAG-NEMO or FLAG-NEMO-Ub_2, were transfected into HEK293T cells and cell lysates (left); anti-NEMO immunoprecipitates (right) were immunoblotted as indicated.

FIGURE 7. Simultaneous recognition of NEMO and ubiquitin by HOIP NZF1 is required for NF-κB activation. (A and B) WT or mutant HOIP NZF1 fused to GST was incubated with K63

diubiquitin (A) or linear tetra-ubiquitin (B) as indicated, followed by pull-down with glutathione beads. Bound proteins were probed as indicated. (C) HA-HOIP or its mutants were transfected into HEK293T cells along with Myc-HOIL-1L, T7-SHARPIN, and FLAG-NEMO, and cell lysates (left) and anti-FLAG immunoprecipitates (right) were immunoblotted as indicated. (D) Full-length NEMO fused with MBP was incubated with K63-diubiquitin and GST-NZF1, followed by pull-down with maltose resins. Bound proteins were probed as indicated. (E) Luciferase activities in HEK293T cells expressing HA-HOIP WT or mutants, along with Myc-HOIL-1L, T7-SHARPIN, and 5× NF-κB luciferase reporter, are shown relative to the activity in cells expressing LUBAC WT, defined as 100% (mean ± SEM; n=3). (F and G) HOIP Δlinear MEFs retrovirally expressing HOIP WT, ΔNZF1, R369A (F) or T354A/F355A (G) were treated with TNF-α (3 ng/ml) for the indicated periods and probed with the indicated antibodies. (H) HOIP Δlinear MEFs retrovirally expressing HOIP WT, ΔNZF1, R369A or T354A/F355A were treated with FLAG-His_6-TNF-α (FH- TNF-α) (3 μg/ml) for the indicated periods; cell lysates (bottom) and anti-FLAG immunoprecipitates (top) were immunoblotted as indicated.

FIGURE 8. Schematic representation of LUBAC-mediated IKK and NF-κB activation. Upon ligand stimulation, LUBAC is recruited to the receptor via the ubiquitin-binding ability of HOIP NZF1. Then, HOIP NZF1 also recognizes NEMO, and this recognition is involved in linear polyubiquitination of NEMO. Linear chains conjugated to NEMO are recognized by NEMO *in*

844 *trans* on another IKK complex, thereby inducing multimerization of the IKK complex and *trans*

845 auto-phosphorylation of IKK2.

Table 1. Data collection and refinement statistics.

	NEMO CoZi/HOIP NZF1 complex
Data collection	
Space group	$P6_5$
Cell dimensions	
a, *b*, *c* (Å)	81.46, 81.46, 74.57
α, *β*, *γ* (°)	90.00, 90.00, 120.00
Wavelength (Å)	1.282
Resolution (Å)	33.0–2.00 (2.05–2.00)[a]
R_{merge}	0.14 (1.11)
$I/\sigma I$	7.7 (1.1)
Completeness (%)	83.1 (66.6)
Redundancy	7.6 (6.8)
CC ½	0.99 (0.63)
Refinement	
Resolution (Å)	50.00–2.00
No. reflections	17945
R_{work}/R_{free} [b]	25.9/31.3
No. atoms	1,743
Protein	1,642
Water	100
Ion	1
B-factors	
Protein	34.4
Water	36.6
Ion	20.6
R.m.s. deviation	
Bond lengths (Å)	0.011
Bond angles (°)	1.369
Ramachandran Statistics	
Residues in most favored regions	97.3%
Residues in additionally allowed regions	2.7%
Residues in generously allowed regions	0.0%

Residues in disallowed regions	0.0%

[a]The values in parenthesis relate to the highest-resolution shells. [b]R_{free} was calculated for a randomly chosen 5% of reflections; the R factor was calculated for the remaining 95% of reflections.

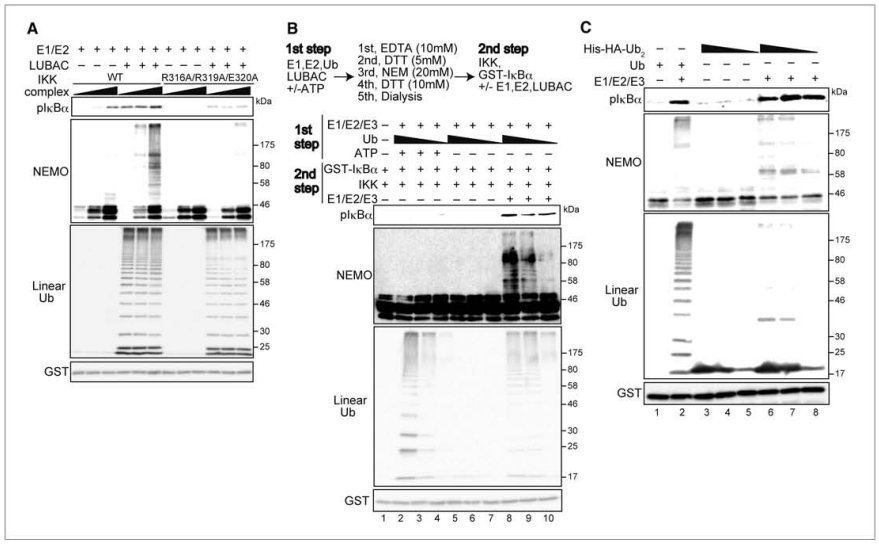

FIGURE1

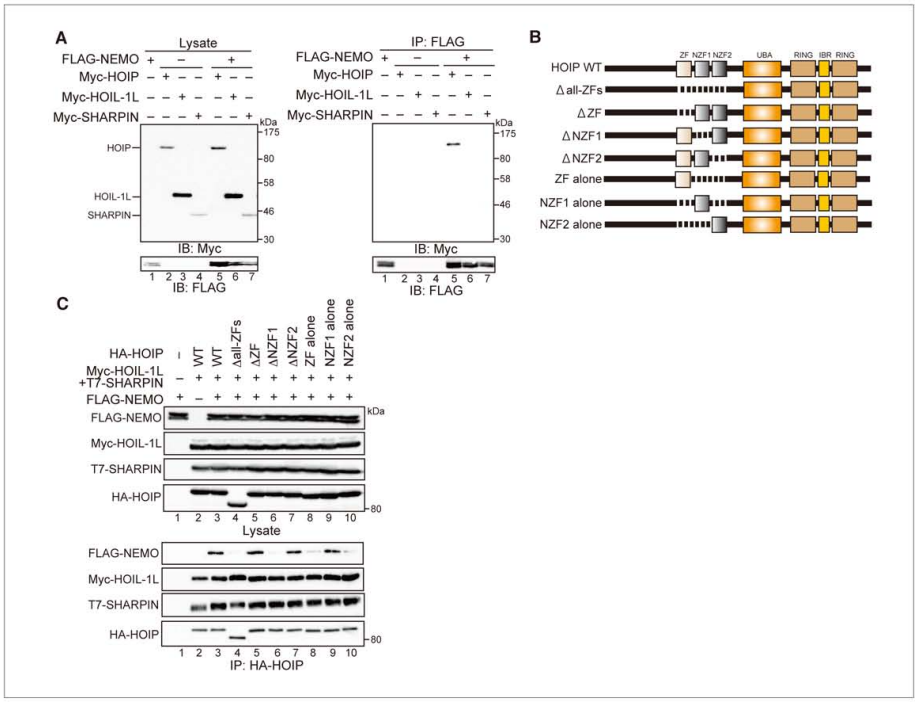

FIGURE2

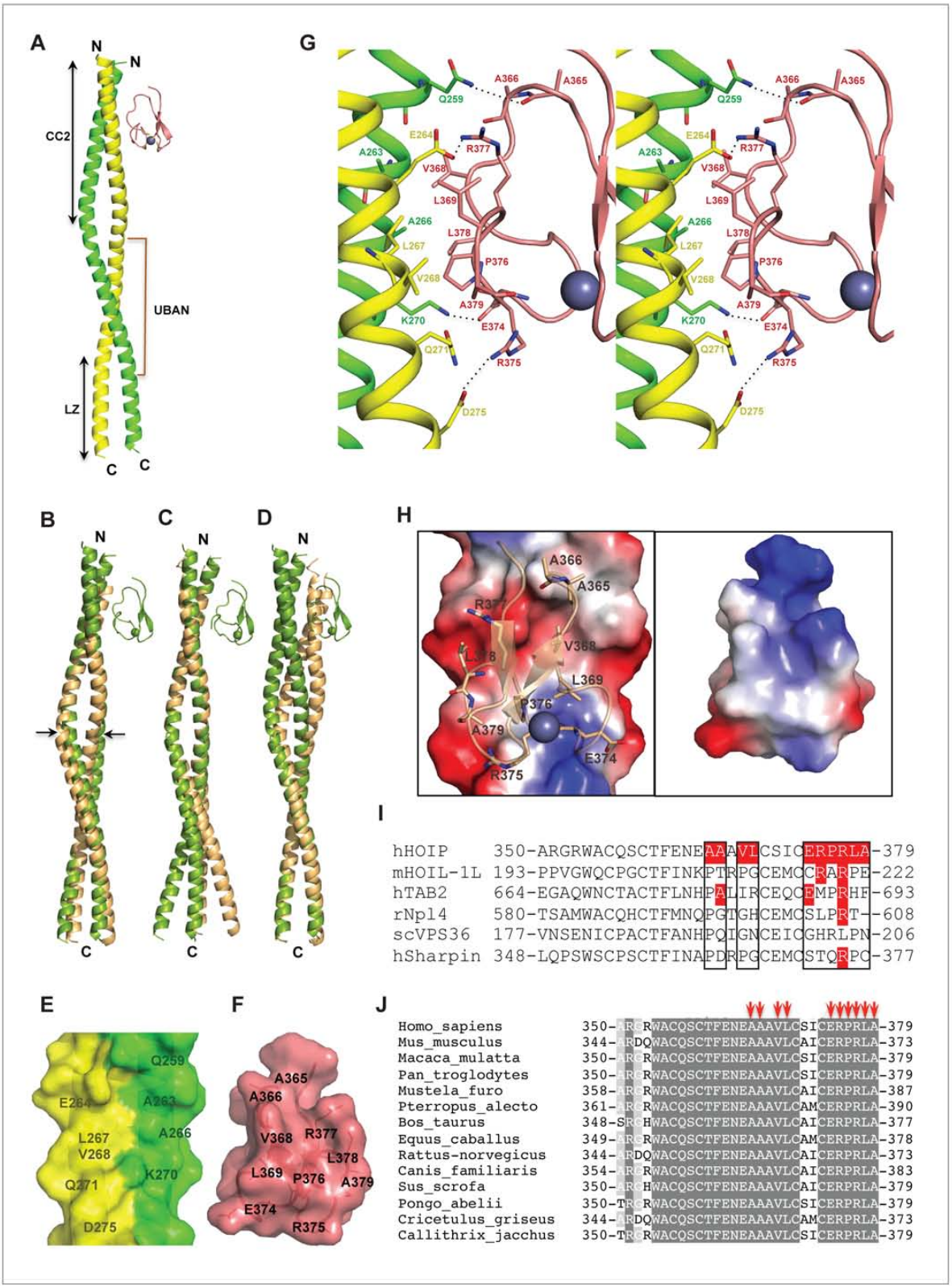

FIGURE3

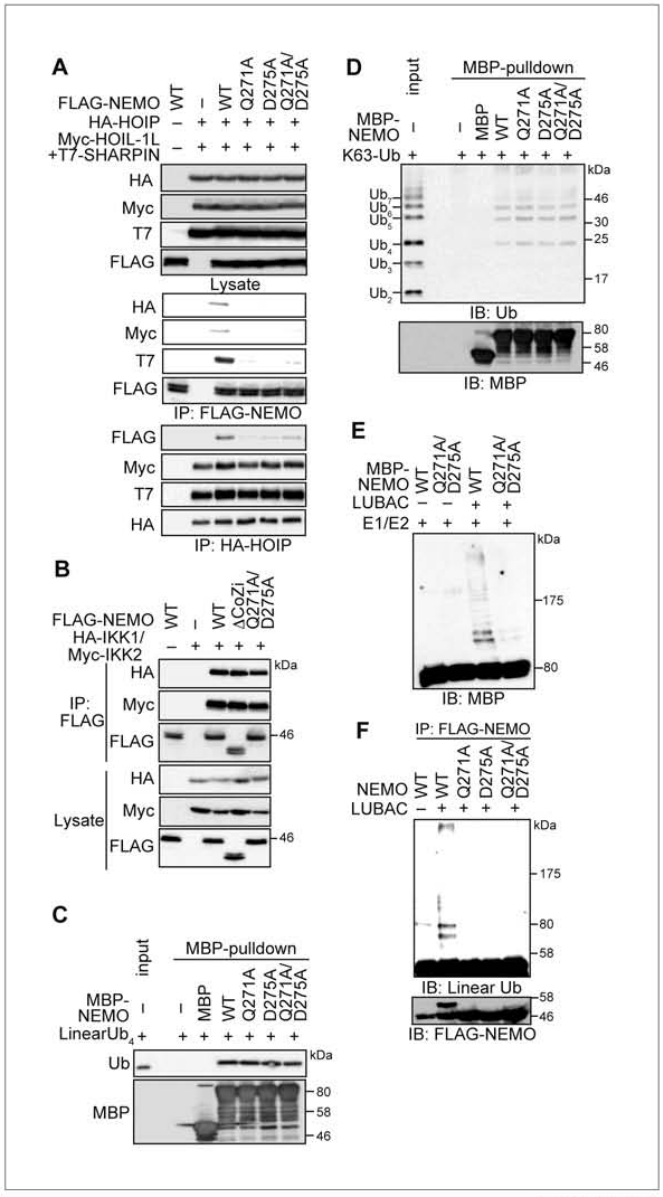

FIGURE4

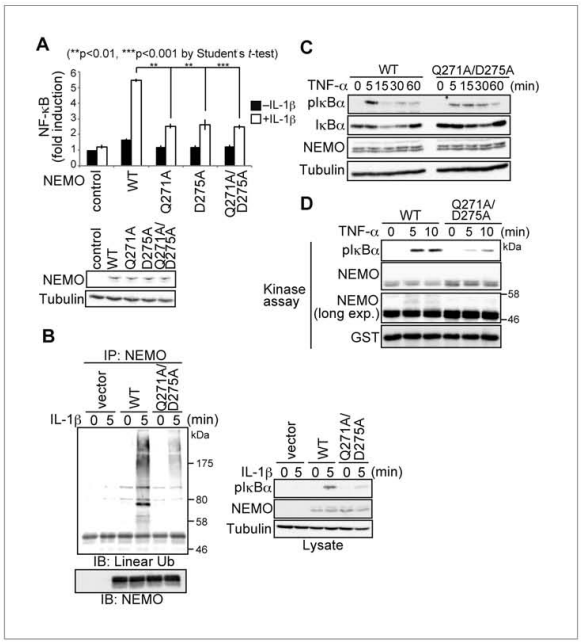

FIGURE5

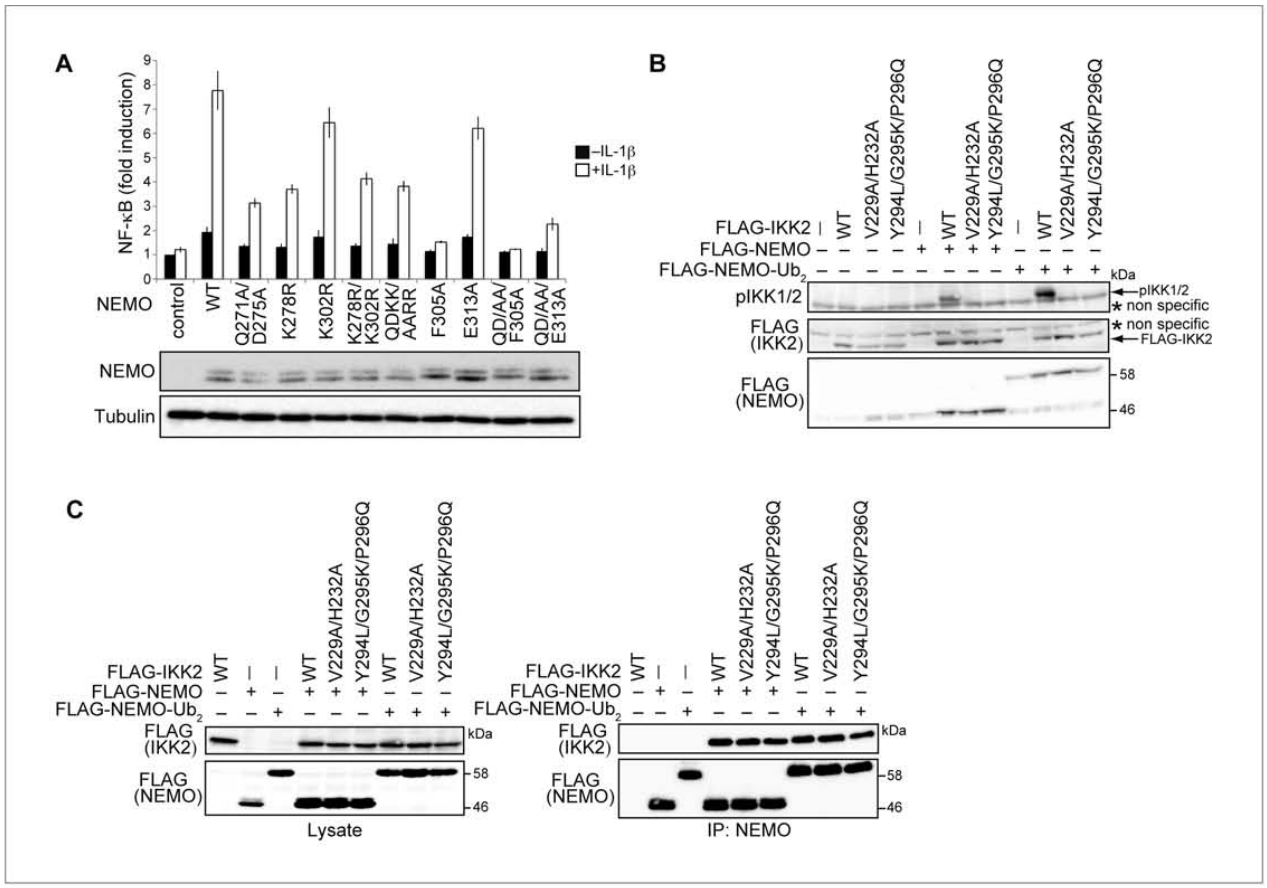

FIGURE6

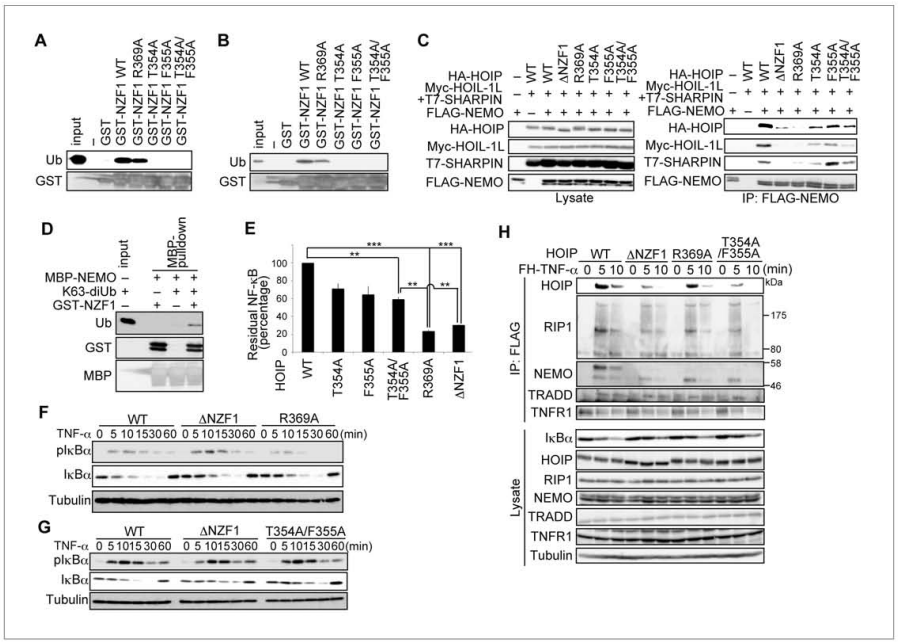

FIGURE7

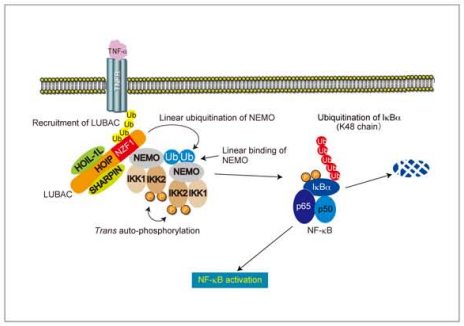

FIGURE8